QuPath Digital Immunohistochemical Analysis of Placental Tissue

Ashley L. Hein

Maheswari Mukherjee

Geoffrey A. Talmon

Sathish Kumar Natarajan

Tara M. Nordgren

See next page for additional authors

Authors

Ashley L. Hein, Maheswari Mukherjee, Geoffrey A. Talmon, Sathish Kumar Natarajan, Tara M. Nordgren, Elizabeth Lyden, Corrine K. Hanson, Jesse L. Cox, Annelisse Santiago-Pintado, Mariam A. Molani, Matthew Van Ormer, Maranda Thompson, Melissa K. Thoene, Aunum Akhter, Ann Anderson-Berry, and Ana G. Yuil-Valdes

QuPath Digital Immunohistochemical Analysis of Placental Tissue

Ashley L. Hein[1], Maheswari Mukherjee[2], Geoffrey A. Talmon[1], Sathish Kumar Natarajan[3], Tara M. Nordgren[4], Elizabeth Lyden[5], Corrine K. Hanson[6], Jesse L. Cox[1], Annelisse Santiago-Pintado[1], Mariam A. Molani[7], Matthew Van Ormer[8], Maranda Thompson[8], Melissa Thoene[8], Aunum Akhter[9], Ann Anderson-Berry[8], Ana G. Yuil-Valdes[1]

[1]Department of Pathology and Microbiology, College of Medicine, University of Nebraska Medical Center, Omaha, NE, USA, [2]Department of Medical Sciences, College of Allied Health Professions, University of Nebraska Medical Center, Omaha, NE, USA, [3]Department of Nutrition and Health Sciences, University of Nebraska-Lincoln, Lincoln, NE, USA, [4]Division of Biomedical Sciences, School of Medicine, University of California Riverside, Riverside, CA, USA, [5]Department of Biostatistics, College of Public Health, University of Nebraska Medical Center, Omaha, NE, USA, [6]Division of Medical Nutrition Education College of Allied Health Professions, University of Nebraska Medical Center, Omaha, NE, USA, [7]University of Texas-Southwestern Medical Center, Dallas, TX, USA, [8]Department of Pediatrics, College of Medicine, University of Nebraska Medical Center, Omaha, NE, USA, [9]Department of Pediatrics, College of Medicine, University of Michigan, Ann Arbor, MI, USA

Abstract

Background: QuPath is an open-source digital image analyzer notable for its user-friendly design, cross-platform compatibility, and customizable functionality. Since it was first released in 2016, at least 624 publications have reported its use, and it has been applied in a wide spectrum of settings. However, there are currently limited reports of its use in placental tissue. Here, we present the use of QuPath to quantify staining of G-protein coupled receptor 18 (GPR18), the receptor for the pro-resolving lipid mediator Resolvin D2, in placental tissue. **Methods:** Whole slide images of vascular smooth muscle (VSM) and extravillous trophoblast (EVT) cells stained for GPR18 were annotated for areas of interest. Visual scoring was performed on these images by trained and in-training pathologists, while QuPath scoring was performed with the methodology described herein. **Results:** Bland–Altman analyses showed that, for the VSM category, the two methods were comparable across all staining levels. For EVT cells, the high-intensity staining level was comparable across methods, but the medium and low staining levels were not comparable. **Conclusions:** Digital image analysis programs offer great potential to revolutionize pathology practice and research by increasing accuracy and decreasing the time and cost of analysis. Careful study is needed to optimize this methodology further.

Keywords: Digital pathology, G-protein coupled receptor 18, image analysis, placenta, QuPath, whole slide image

INTRODUCTION

The field of pathology is becoming increasingly computerized. Starting in the late 1990s, the first digital slide scanners became commercially available, which led to increased opportunities for slide sharing and teaching and ultimately fueled the evolution of software with the ability to perform complex analyses such as digital image analysis of immunohistochemistry (IHC)-stained slides.[1,2]

There are many digital image analyzers (DIAs) with unique functionality currently on the market. Some examples of open-source programs include Image J, Fiji, Icy, CellProfiler, and QuPath. QuPath is an open-source software for whole slide image analysis that, unlike most other DIAs, has been designed to easily handle large two-dimensional images up

to 40 gigabytes (GB) in size.[3] It is a multithreaded DIA that has numerous annotation tools and can be customized to perform more complex tasks. It is notable for its user-friendly design and is modifiable so that it may become compatible with other DIAs, addressing the common problem of limited cross-platform interoperability. QuPath has been applied in over 624 publications since it was first released in 2016[3] including applications in the identification

Access this article online

Quick Response Code:

Website:
www.jpathinformatics.org

DOI:
10.4103/jpi.jpi_11_21

of various biomarkers in colon adenocarcinoma, renal tissue, uveal melanoma, breast cancer, non-small cell lung cancer, ovarian carcinoma, and neural tissue.[4-11] However, there are currently limited reports of its use in placental tissue,[12-14] with those reports largely consisting of analyses of inflammatory cell populations with minimal descriptions of analyses of placental and vascular tissue.[15-17] G-protein coupled receptor 18 (GPR18) is the receptor for Resolvin D2, a pro-resolving lipid mediator recently identified as providing a protective benefit to placental cells against inflammatory processes.[18] Previous studies of this receptor have shown its consistent membranous and cytoplasmic expression in vascular smooth muscle (VSM) and extravillous trophoblast (EVT) cells in placental tissue, leading to its selection for this analysis.

Herein, we report the methodology and findings from our study, where we compare QuPath and traditional visual analysis ability to score GPR18 staining in VSM and EVT in placental tissue.

METHODS

Development of the study
This study received Institutional Review Board approval from the University of Nebraska Medical Center. Cross-sections were collected from 20 full-term third-trimester placentas from unremarkable pregnancies, fixed in 10% formalin, and then embedded in paraffin. Traditional glass slides were prepared by obtaining 4 µ thick tissue sections. Once the glass slides were prepared, IHC staining for GPR18 (polyclonal; Thermo Fischer Scientific; 1:75 dilution) was performed using standard autostaining protocols on a Ventana Discovery Ultra autostainer.

The IHC-stained glass slides were then digitized at a single focal plane level with ×40 magnification, and the resulting image was stored in bif format using a VENTANA iScan HT scanner. The digital images were stored in two separate encrypted and password-protected external hard drives, A and B. The set of images in hard drive A was used to analyze VSM cells and the set of images in hard drive B was used to analyze EVT cells.

To analyze vascular smooth muscle
Tissue slides with at least ten blood vessels were selected to further quantify the percentage (0%–100%) and intensity (low vs. medium vs. high) of GPR18 immunoreactivity, resulting in ten digital images for the analyses.

To analyze extravillous trophoblast cells
Tissue slides with at least 100 cells were selected to further quantify the percentage (0%–100%) and intensity (low vs. medium vs. high) of GPR18 immunoreactivity, resulting in ten digital images for the analyses.

VSM and EVT were annotated (digitally marked) in ten digital images using VENTANA Image Viewer software (version 3.1.3;

Roche, Indianapolis, IN, USA), a web-based application by BioImagene.

Data collection
Four participants (two pathologists and two pathology residents) each performed visual analysis of all twenty digital images (VSM and EVT) and four participants (one pathologist, one cytotechnologist, one pediatrics resident, and one medical student) each performed QuPath analysis of all twenty digital images (VSM and EVT).

Manual scoring method
- The study participants were given a brief training session on how to access the digital images saved on the encrypted external hard drive and how to use the Image Viewer software to screen the digital images
- The participants were asked to visually interpret the preannotated digital images and provide their interpretations for the percentage (0%–100%) and intensity (low, 1+; medium, 2+; and high, 3+) of the IHC staining for each image
- All participants independently interpreted the digital images using their personal workstations and computer monitors.

QuPath scoring method
- The participants downloaded QuPath version 0.1.2 with the minimum RAM requirement of 8 GB onto their personal computers. As per system requirements, the computers used were either 64-bit processors or OSx10.7.4 or above with at least 500 megabytes (MB) of hard disk space
- The participants were then given a flow chart and an in-person tutorial regarding the analysis of the digital images using QuPath software
- The digital image files were downloaded into the QuPath software
- The image type of brightfield (H-DAB) was selected with ×40 magnification and 0.25 µm pixels. For IHC analysis, the image type was changed from H and E to DAB to reflect the chromogen used for immunostaining. In addition, the higher magnification was chosen because it provided higher pixelation and more detail
- Using the preannotated digital images from the hard drive as references, the polygon tool was used to select the region of interest for analysis. The EVT and VSM stained with GPR18 were annotated and analyzed separately
- Before running the analyses, optimal stain separation in brightfield images was obtained by first estimating the stain vectors. This method was performed by choosing the "estimate stain vectors" command under the "analyze" menu in the QuPath software
- The analyses were performed using cell analysis and positive cell detection with the setup parameters that are shown in Table 1. The single threshold option was inactivated because this was a multiple intensity analysis. The cutoff thresholds for 1+, 2+, and 3 + were determined

Table 1: Positive cell detection parameters

Setup parameters	Detection image	Optical density sum (0.2 μm)
	Requested pixel	
Nucleus parameters	Background radius	8 μm
	Median filter radius	1.5 μm
	Sigma	3.5 μm (VSM)
		3.0 μm (EVT)
	Minimum area	10 μM²
	Maximum area	400 μM²
Intensity parameters	Threshold	0.05
	Max background intensity	2
	Split by shape	Yes
	Exclude DAB (membrane staining)	No
Cell parameters	Cell expansion	5 μm
	Include cell nucleus	Yes
General parameters	Smooth boundaries	Yes
	Make measurements	Yes
Intensity threshold parameters	Score compartments	Cell: DAB OD mean
	Threshold 1+	0.05
	Threshold 2+	0.1
	Threshold 3+	0.2
	Single threshold	No

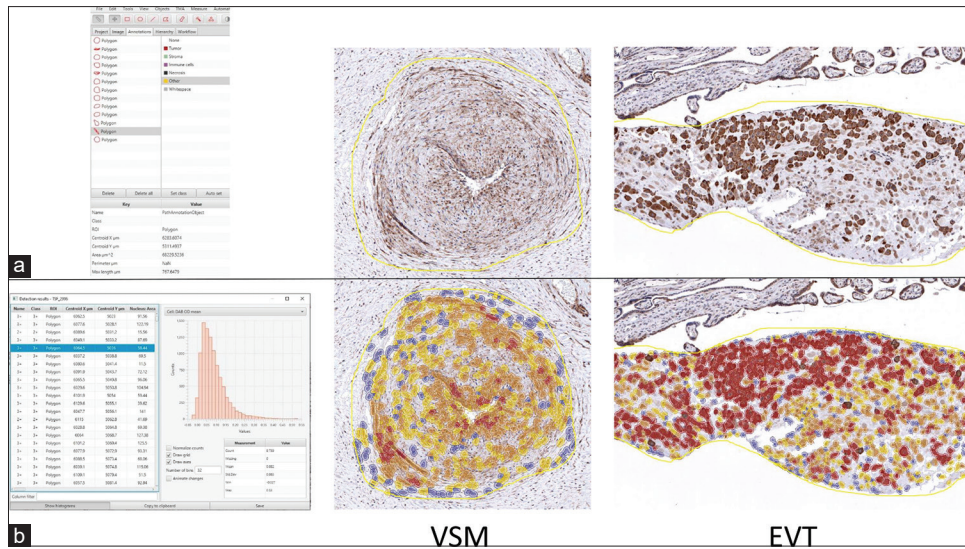VSM: Vascular smooth muscle, EVT: Extravillous trophoblast

Figure 1: QuPath measurement map tool. (a) QuPath measurement map tool being used to adjust staining threshold parameters. (b) Representative images show how QuPath's measurement map tool was used to visualize individual cell staining intensities for the indicated placental tissues

before the analysis by one pathologist using QuPath heat maps. "Cell: DAB OD mean" was used for the analysis as both membranous and cytoplasmic staining of a selective antibody was being performed. To analyze cytoplasmic staining alone, an option would be to use "Cytoplasm: DAB OD mean"

- The "measurement map" tool, as shown in Figure 1, was utilized to visualize stain intensity across the annotations and was used to adjust the GPR18 intensity threshold parameters. This option, accessed under the "measure" menu, provides a color-coded representation where each cell's color reflects the intensity of DAB staining within that cell. Any cutoff thresholds were checked visually
- After clicking "run," the software performed the digital analysis, and the results and histograms were reviewed under annotation measurements. Figure 2 shows representative images of analyses, showing the use of the polygon tool and the final analysis with a histogram and cells sorted by intensity.

Statistical analysis

Assessment of agreement between visual and QuPath data by type of image (VSM or EVT) and staining category (low, medium, or high) was performed using a Bland–Altman (BA) comparison and visualized with BA plots. For each slide for VSM and EVT, at each level (low, medium, and high), the average intensity given by the four participants using the visual method, and the average intensity from the four participants using the QuPath method was determined. These average intensities are visualized on the BA plot, with each plot consisting of 10 points representing the 10 slides that were evaluated. Included on each plot is the y-axis line, which represents the mean of differences and the limits of agreement

lines: mean +2 standard deviations (SDs) and mean −2 SDs. Mean differences and SDs between image analysis methods were used as descriptive statistics. In addition, data were converted into H-scores. The average H-Score of the four participants using the visual method was determined for each of the ten digital images. Similarly, the average H-Score of the four participants using the QuPath method was determined. Spearman correlations and scatterplots were used to evaluate the correlation between the 10 average H-scores (i.e., mean of four participants for each digital image) and the visual method with the 10 average H-scores from the QuPath method for EVT and VSM. All analyses were done using SAS 9.4.

RESULTS

As seen in Figure 3, for VSM, the average of the differences and SD between the two image analysis methods for low, medium, and high intensity were 11.23 (20.70), −13.79 (11.00), and 2.57 (14.45), respectively. For low intensity, this suggests that on average estimates of visual intensity for visual were 11.23% higher than that for QuPath, while for the medium category, the average visual intensity was 13.79% lower than QuPath, and for high visual average intensity was 14.45% higher than QuPath. Average values of percent intensity for each slide, by intensity category, are visualized as dots on BA plots. For VSM, all points lie within two SDs of the mean, suggesting that the two methods are comparable for VSM at low, medium, and high intensities.

As seen in Figure 4, for EVT, the average of the differences and SD between the two image analysis methods for low, medium, and high intensity was 3.08 (28.85), 4.86 (28.83), and −8.31 (16.54), respectively. For low intensity, this suggests that on average estimates of intensity for visual were 3.08% higher than that for QuPath, while for medium visual average intensity was 4.86% higher than QuPath, and for high visual average intensity was 8.31% lower than QuPath. Average values of percent intensity for each slide, by intensity category, are visualized as dots on BA plots. For EVT at high staining intensity, all data points were within 2 SDs of the mean, suggesting that for EVT at high staining intensity, the two methods are comparable. For EVT at low and medium

Figure 2: QuPath analysis polygon tool. (a) Left: QuPath annotation toolbox with polygon tool selected. Right: Representative images show how QuPath's polygon tool was used to select either vascular smooth muscle or extravillous trophoblast as the region of interest for analysis. (b) Left: A histogram indicates the staining intensities for all cells within annotated areas for one specimen. Right: Representative images show cell staining intensity for the indicated G-protein coupled receptor 18 stained placental tissues. Cell staining intensity is represented as follows: negative (blue), low (yellow), medium (orange), and high (red)
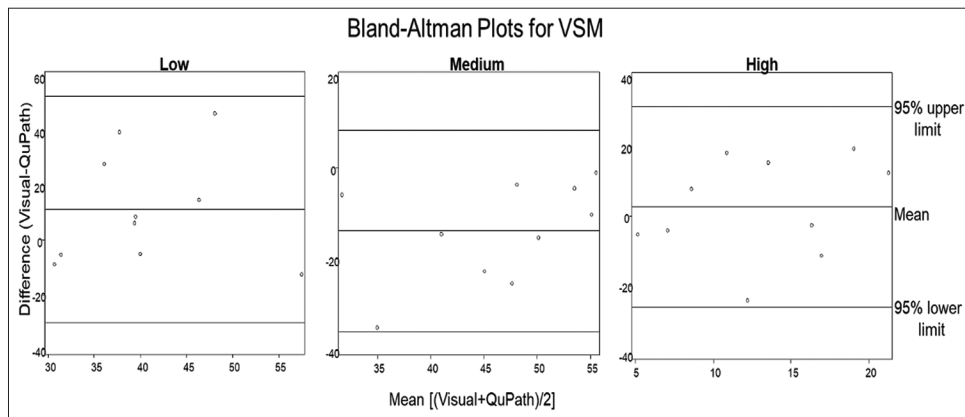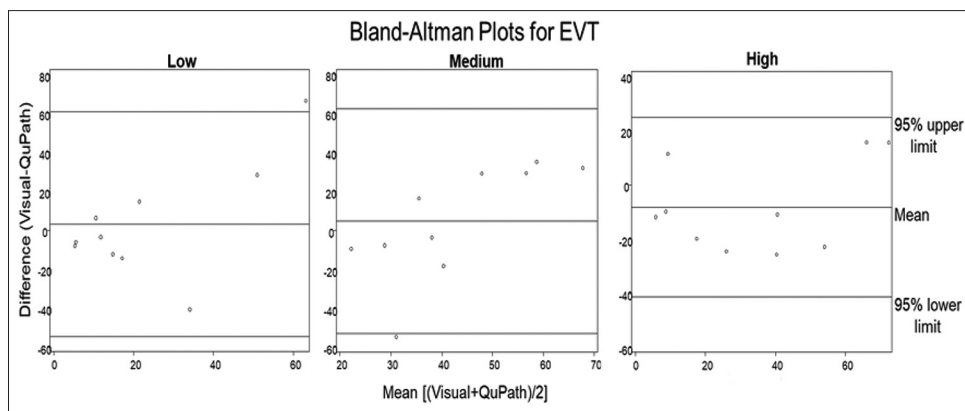

Figure 3: Bland–Altman plots for vascular smooth muscle. Comparison of average of the difference and mean difference of staining intensity percentage between visual scoring and QuPath for vascular smooth muscle low, medium, and high staining categories. Comparison of scoring methods between low, medium, and high-intensity staining produced average differences and standard deviations of 1.23 (20.70), −13.79 (11.00), and 2.57 (14.45), respectively. All data points were within 2 standard deviations (95% confidence interval) of the mean

staining intensity, each has one data point that lies outside of two SDs of the mean, suggesting that the two methods are not comparable for EVT at this staining intensity. For the EVT low category, one data point was outside of 2 SDs. For this data point, pathologists estimated that 90%–100% of this slide stained low intensity, while QuPath estimated that 14%–40% of the cells were in the low-intensity staining category. Similarly, for the EVT medium category, one data point is outside of 2 SDs. Visual methods estimated 0%–10% of cells stained in the medium category, while QuPath estimated that 50%–71% of cells stained in the medium category. Of interest is the fact that these values were both taken from the same slide image: EVT Slide #10. Upon review, EVT Slide #10 was noted to contain a significant folding artifact.

Figure 5 displays a scatterplot comparing the two methods by H-score for VSM. There was no statistically significant correlation between H-scores for the visual and QuPath methods for VSM ($r = −0.33$, $P = 0.35$). There was a statistically significant correlation between H-scores for the visual and QuPath methods for EVT ($r = 0.88$, $P = 0.0009$) as shown in Figure 6. This discrepancy between results by BA analysis and Spearman correlation can be explained by the fact that the data were analyzed by intensity levels in the former and H-scores in the latter.

DISCUSSION

While the reference standard for the determination of IHC staining continues to be visual scoring by trained

Figure 4: Bland–Altman plots for extravillous trophoblast. Comparison of average of the difference and mean difference of staining intensity percentage between visual scoring and QuPath for extravillous trophoblast low, medium, and high staining categories. Comparison of scoring methods between low, medium, and high-intensity staining produced average differences and standard deviations of 3.08 (28.85), 4.86 (28.83), and -8.31 (16.54), respectively. All data points for high intensity were within 2 standard deviations (95% confidence interval) of the mean, while low and medium categories each had one data point outside of 2 standard deviations
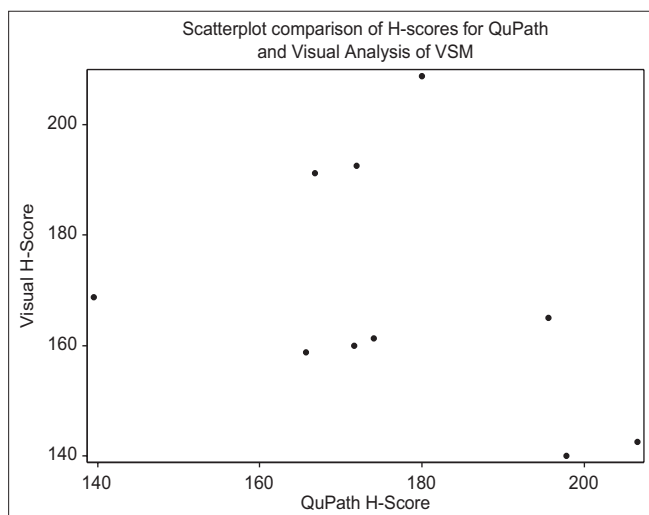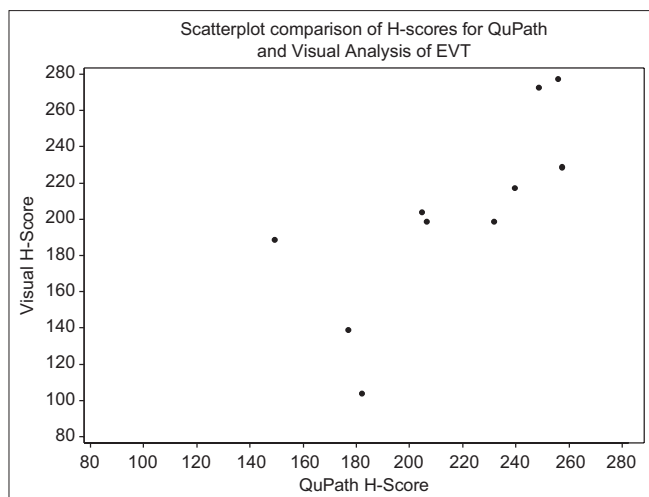

Figure 5: Scatterplot comparison of H-scores for QuPath and visual analysis of vascular smooth muscle. The average H-score for each image by method is shown in this scatterplot. Spearman correlation was performed and revealed no statistically significant correlation between the H-score for the visual method and the H-score for the QuPath method ($r = -0.33, P = 0.35$)

pathologists,[19-21] DIAs offer many benefits over traditional scoring. Two common systems of visual scoring include H scoring and the Allred score.[21] With both of these methods, tissues are assigned a percent score for categories of staining intensity such as none, low, medium, and high. This creates ordinal (semiquantitative) data. DIAs allow for the creation of quantitative instead of ordinal data, producing rigorous results with more precise, linear correlations to biological and clinical outcomes.[4,22-24] Another limitation of visual scoring is that the data produced are affected by human sources of both cognitive and visual bias.[19] Visual traps, or optical illusions, cause the perception of an image to differ from its reality with examples including the illusion of size, lateral inhibition, and individual variability in the perception of color

gradients. Cognitive traps are biases in thought patterns and can include confirmation bias, avoidance of extreme ranges, and number preference, all of which can affect IHC scoring. The use of DIAs provides objective analyses that can increase reproducibility and accuracy of scoring by reducing sources of human errors. In addition, the use of a pathologist to score slides may increase the cost, as well as the time of analysis, as there are free open-source DIAs available that can analyze large sets of data faster than can be performed manually.[5,21,24] The time of analysis is also improved by the fact that individuals without an extensive pathology background can perform QuPath analysis. Pathologists and researchers can use this DIA methodology without image analysis and programming expertise. This technique can be incorporated into research with different human tissues or animal models, allowing for a more rapid return of results. In addition, DIAs can be standardized, enabling pathologists and researchers to work together in clinical and translational research.

Our study analyzed placental tissue, a vastly underutilized resource. Research of this organ has the potential to provide insight into the pathophysiology of placental dysfunction, allowing for the early diagnosis and prevention of placenta-mediated pregnancy complications. Our research and analysis of GPR18 expression in human placental tissue will help uncover the role of pro-resolving lipid mediators against inflammation and vascular injury in pregnancy and perinatal disease.

The goal of the current study was to compare traditional visual scoring with that of the open-source digital image analysis program QuPath in placental tissue. The discrepancy between the results seen by Spearman correlation and the BA plot can be explained by the fact that the former utilized H-scores while the latter analyzed by intensity staining categories. The H-score is heavily influenced by the predominant staining intensity. Analysis by intensity staining category allows for a more detailed analysis of the accuracy of QuPath grading.

Figure 6: Scatterplot comparison of H-scores for QuPath and visual analysis of extravillous trophoblast. The average H-score for each image by method is shown in this scatterplot. Spearman correlation was performed and revealed a statistically significant correlation between the H-score for the visual method and the H-score for the QuPath method ($r = 0.88$, $P = 0.0009$)

A BA analysis was selected to demonstrate comparability between the two methods. The BA plots allow for the visualization of systematic differences between the methods and possible outliers in the image analysis. For VSM and the EVT high-intensity staining category, the two methods were comparable by BA analysis.

Furthermore, while visual analyses were performed by trained and in-training pathologists, the QuPath analyses were performed by individuals with a range of different levels of expertise, showing overall data congruity and supporting QuPath as a user-friendly DIA capable of great accuracy.

For the EVT low and medium categories, each had a data point that existed outside of 2 SDs. These differences can likely be explained by the folding artifacts present in EVT Slide #10. While a pathologist would account for folding artifacts in their visual scoring, analysis of the same slide by a DIA results in oversegmentation, where cells are erroneously subdivided, resulting in a greater number of calculated cells than would otherwise have been expected. Segmentation is a common problem among DIAs with sensitivity, specificity, contour accuracy, and segmentation accuracy needing to be balanced.[25] Another possible explanation for these differences could be that QuPath picked up on "subvisual" differences within the slide that were not visible to the naked eye, a characteristic that has been ascribed to DIAs before.[26,27] While the minimum specifications for this version of QuPath were used, a more efficient and uniform performance could have been achieved by meeting the recommended specifications including using 16GB of RAM, a discrete graphics card, solid-state hard disk, multicore processor, and 1GB or greater of hard disk space per slide.[28] Since personal computers were used for these analyses, the type of processor, graphics

abilities, and hard disk space varied. Finally, this study did have the limitation of a small sample size. Additional studies are needed with data collected from more participants to further evaluate the reproducibility of the results and to increase the power of this study.

CONCLUSIONS

As shown in this study, QuPath's ease of access, user-friendly design, and accuracy demonstrates the potential for this software in future research and clinical applications.

Financial support and sponsorship

Conflicts of interest

There are no conflicts of interest.

REFERENCES

1. Pantanowitz L, Sharma A, Carter AB, Kurc T, Sussman A, Saltz J. Twenty years of digital pathology: An overview of the road travelled, what is on the horizon, and the emergence of vendor-neutral archives. J Pathol Inform 2018;9:40.
2. Bacus JV, Bacus JW. Method and Apparatus for Acquiring and Reconstructuring Magnified Specimen Images from a Computer-Controlled Microscope. Bacus Laboratories Inc. US Patent 6226392B1 filed 1998 Mar 02, and granted 2007 Aug 22.
3. GitHub. Citing QuPath. QuPath Website. Available from: https://github.com/qupath/qupath/wiki/Citing-QuPath. [Last accessed on 2021 May 21; Last updated on 2021 May 18].
4. Bankhead P, Loughrey MB, Fernández JA, Dombrowski Y, McArt DG, Dunne PD, et al. QuPath: Open source software for digital pathology image analysis. Sci Rep 2017;7:16878.
5. Stålhammar G, See TR, Phillips S, Seregard S, Grossniklaus HE. Digital image analysis of BAP-1 accurately predicts uveal melanoma metastasis. Transl Vis Sci Technol 2019;8:11.
6. Ribeiro GP, Endringer DC, De Andrade TU, Lenz D. Comparison between two programs for image analysis, machine learning and subsequent classification. Tissue Cell 2019;58:12-6.
7. Humphries MP, Hynes S, Bingham V, Cougot D, James J, Patel-Socha F, et al. Automated tumour recognition and digital pathology scoring unravels new role for PD-L1 in predicting good outcome in ER-/HER2+breast cancer. J Oncol 2018;2018:2937012.
8. Ledys F, Klopfenstein Q, Truntzer C, Arnould L, Vincent J, Bengrine L, et al. RAS status and neoadjuvant chemotherapy impact CD8+ cells and tumor HLA class I expression in liver metastatic colorectal cancer. J Immunother Cancer 2018;6:123.
9. Haragan A, Field JK, Davies MP, Escriu C, Gruver A, Gosney JR. Heterogeneity of PD-L1 expression in non-small cell lung cancer: Implications for specimen sampling in predicting treatment response. Lung Cancer 2019;134:79-84.
10. Hollis RL, Carmichael J, Meynert AM, Churchman M, Hallas-Potts A, Rye T, et al. Clinical and molecular characterization of ovarian carcinoma displaying isolated lymph node relapse. Am J Obstet Gynecol 2019;221:245.e1- 245.e15.
11. Morriss NJ, Conley GM, Ospina SM, Meehan Iii WP, Qiu J, Mannix R. Automated quantification of immunohistochemical staining of large animal brain tissue using qupath software. Neuroscience 2020;429:235-44.
12. Cizkova K, Foltynkova T, Gachechiladze M, Tauber Z. Comparative analysis of immunohistochemical staining intensity determined by light microscopy, imagej and qupath in placental hofbauer cells. Acta Histochem Cytochem 2021;54:21-9.
13. Bezemer RE, Schoots MH, Timmer A, Scherjon SA, Erwich JJ, van Goor H, et al. Altered levels of decidual immune cell subsets in fetal

growth restriction, stillbirth, and placental pathology. Front Immunol 2020;11:1898.

14. Kerby A, Shingleton D, Batra G, Sharps MC, Baker BC, Heazell AE. Placental morphology and cellular characteristics in stillbirths in women with diabetes and unexplained stillbirths. Arch Pathol Lab Med 2021;145:82-9.

15. Kretschmer T, Turnwald EM, Janoschek R, Zentis P, Bae-Gartz I, Beers T, *et al*. Maternal high fat diet-induced obesity affects trophoblast differentiation and placental function in mice†. Biol Reprod 2020;103:1260-74.

16. Shawer H, Aiyelaagbe E, Clowes C, Lean SC, Lu Y, Kadler KE, *et al*. A missense mutation of ErbB2 produces a novel mouse model of stillbirth associated with a cardiac abnormality but lacking abnormalities of placental structure. PLoS One 2020;15:e0233007.

17. Tsunoda Y, Kudo M, Wada R, Ishino K, Kure S, Sakatani T, *et al.* Expression level of long noncoding RNA H19 of normotensive placentas in late pregnancy relates to the fetal growth restriction. J Obstet Gynaecol Res 2020;46:1025-34.

18. Ulu A, Sahoo PK, Yuil-Valdes AG, Mukherjee M, Van Ormer M, Muthuraj PG, *et al*. Omega-3 fatty acid-derived resolvin D2 regulated human placental vascular smooth muscle extravillous trophoblast activities. Int J Mol Sci 2019;20:4402.

19. Aeffner F, Wilson K, Martin NT, Black JC, Hendriks CLL, Bolon B, *et al.* The gold standard paradox in digital image analysis: Manual versus automated scoring as ground truth. Arch Pathol Lab Med 2017;141:1267-75.

20. Daunoravicius D, Besusparis J, Zurauskas E, Laurinaviciene A, Bironaite D, Pankuweit S, *et al*. Quantification of myocardial fibrosis by digital image analysis and interactive stereology. Diagn Pathol 2014;9:114.

21. Varghese F, Bukhari AB, Malhotra R, De A. IHC Profiler: An open source plugin for the quantitative evaluation and automated scoring of immunohistochemistry images of human tissue samples. PLoS One 2014;9:e96801.

22. Taylor CR, Levenson RM. Quantification of immunohistochemistry – Issues concerning methods, utility and semiquantitative assessment II. Histopathology 2006;49:411-24.

23. Bankhead P, Fernández JA, McArt DG, Boyle DP, Li G, Loughrey MB, *et al.* Integrated tumor identification and automated scoring minimizes pathologist involvement and provides new insights to key biomarkers in breast cancer. Lab Invest 2018;98:15-26.

24. Meyerholz DK, Beck AP. Principles and approaches for reproducible scoring of tissue stains in research. Lab Invest 2018;98:844-55.

25. Aeffner F, Zarella MD, Buchbinder N, Bui MM, Goodman MR, Hartman DJ, *et al.* Introduction to digital image analysis in whole-slide imaging: A white paper from the digital pathology association. J Pathol Inform 2019;10:9.

26. Wang X, Wang D, Yao Z, Xin B, Wang B, Lan C, *et al.* Machine learning models for multiparametric glioma grading with quantitative result interpretations. Front Neurosci 2018;12:1046.

27. Carleton NM, Lee G, Madabhushi A, Veltri RW. Advances in the computational and molecular understanding of the prostate cancer cell nucleus. J Cell Biochem 2018;119:7127-42.

28. GitHub. System Requirements. QuPath Website. Avaialble from: https://github.com/qupath/qupath/wiki/System-requirements. [Last accessed on 2020 Dec 21; Last updated on 2016 Oct 04].